Lattice Effects on the Formation of Oxygen Vacancies in Perovskite Thin Films

Claudio Cazorla

School of Materials Science and Engineering, UNSW Australia, Sydney, New South Wales 2052, Australia and Integrated Materials Design Centre, UNSW Australia, Sydney, New South Wales 2052, Australia

(Received 18 December 2016; revised manuscript received 8 February 2017; published 27 April 2017)

We use first-principles methods to investigate the effects of collective lattice excitations on the formation of oxygen vacancies in perovskite thin films. We find that phonons play a crucial role in the strain-mediated control of defect chemistry at finite temperatures. Specifically, zero-temperature oxygen-vacancy formation trends deduced as a function of epitaxial strain can be fully reversed near room temperature. Our first-principles calculations evidence a direct link between the lattice contribution to the oxygen-vacancy free energy and the volume expansion that the system undergoes when it is chemically reduced: The larger the resulting volume expansion, the more favorable thermal excitations are to point-defect formation. However, the interplay between the vibrational vacancy entropy—or, equivalently, chemical expansion—and epitaxial strain is difficult to generalize, as it can be strongly influenced by underlying structural and magnetic transitions. In addition, we find that vacancy ordering can be largely hindered by the thermal lattice excitations.

DOI: 10.1103/PhysRevApplied.7.044025

I. INTRODUCTION

Point defects can affect considerably the structural, magnetic, and transport properties of perovskite-structure materials with chemical formula ABO_3. Oxygen vacancies (V_O), for example, enable ionic conductivity in perovskite-based solid solutions to be used for electrochemical applications such as solid oxide fuel and electrolysis cells [1–3]. Likewise, V_O can significantly distort the equilibrium arrangement of atoms and hence can modify the superexchange interactions between neighboring magnetic ions [4–6]. The presence of point defects in perovskite oxides also is known to induce an increase of volume, the so-called chemical expansion [7–10]; such an effect is caused by atomic underbonding due to the extra electrons provided by the oxygen vacancies, which are located in nonbonding transition-metal orbitals [Fig. 1(a)]. Engineering of defects in perovskite oxides, therefore, emerges as a likely avenue for the design of new materials with tailored functionality.

Recently, it was experimentally demonstrated that strain engineering can be used to tune the content of oxygen in some perovskite oxides [2,11–14]. For example, in $SrCoO_{3-\delta}$ thin films, a moderate epitaxial strain of about $+2\%$ produces an approximately 30% reduction in the oxygen activation energy barrier, which makes it possible to stabilize oxygen-deficient samples at annealing temperatures close to ambient conditions [12]. Also, in multiferroic $SrMnO_3$ thin films, the formation energy of oxygen vacancies can be decreased by as much as 0.25 eV upon application of an epitaxial strain of about $+4\%$ [13].

First-principles computational methods have been used to unveil the atomistic mechanisms behind strain-mediated V_O formation at zero temperature (i.e., by neglecting possible thermal effects) [15–17]. Interestingly, Aschauer *et al.* [15] showed that the formation energy of oxygen vacancies in $CaMnO_3$ thin films is strongly favored by tensile (positive) epitaxial strain. This finding has been rationalized in terms of general electrostatic arguments based on the fact that the accompanying electron-electron repulsion is effectively reduced along elongated Mn-Mn distances. Nevertheless, experiments performed in $CaMnO_3$ thin films covering a wide range of epitaxial states have not evidenced any preference for V_O formation at tensile conditions [18]. Furthermore, recent measurements in $SrCoO_{3-\delta}$ thin films by Hu *et al.* [14] revealed a nonmonotonic sawtooth dependence of the critical reduction temperature on epitaxial strain, with a marked peak at moderate tensile stresses. Hu *et al.*'s experimental results come to suggest the presence of contributions to V_O formation other than the purely electrostatic.

In this work, we employ first-principles methods based on density-functional theory (DFT) to quantify the effects of thermal lattice excitations on the formation energy of V_O in perovskite thin films. We select $SrCoO_{3-\delta}$ (SCO) and $La_{0.5}Sr_{0.5}Mn_{0.5}Co_{0.5}O_{3-\delta}$ (LSMCO) as the reference systems in which to perform our calculations because they exhibit one of the highest oxygen-deficient stoichiometries observed to date at ambient conditions in a simple perovskite [19–21]. Our computational results show that (1) thermal lattice excitations play a crucial role on the strain dependence of oxygen-vacancy formation, as they can fully reverse the energy trends deduced at zero temperature; (2) the larger the chemical expansion experienced by the system, the more favorable the vibrational entropy is to V_O formation; and (3) the vibrational entropy of oxygen vacancies depends on the defect symmetry, that is, whether

it is equatorial or apical [Fig. 1(b)], which, in some cases, may oppose vacancy ordering.

II. METHODS

A. Free energy of oxygen-vacancy formation

We compute the quasiharmonic Gibbs free energy associated with the formation of neutrally charged oxygen vacancies, $G^{\mathrm{qh}}_{\mathrm{vac}}$, as a function of epitaxial strain, $\eta \equiv (a - a_0)/a_0$ (in all of the cases, a_0 represents the equilibrium in-plane lattice parameter calculated in the stoichiometric system), and temperature, T. This quantity can be expressed as [14]

$$G^{\mathrm{qh}}_{\mathrm{vac}}(\eta, T) = E_{\mathrm{vac}}(\eta) + F^{\mathrm{qh}}_{\mathrm{vac}}(\eta, T) + \mu_{\mathrm{O}}(T), \qquad (1)$$

where the subscript vac indicates the quantity difference between the defective and perfect systems (e.g., in SCO, $A_{\mathrm{vac}} \equiv A_{\mathrm{SrCoO}_{3-\delta}} - A_{\mathrm{SrCoO}_3}$), E_{vac} accounts for the static contributions to the free energy (i.e., calculated at $T = 0$ conditions by considering the atoms fixed at their equilibrium lattice positions), $F^{\mathrm{qh}}_{\mathrm{vac}}$ represents the vibrational contributions to the free energy, and μ_{O} is the chemical potential of the free oxygen atom. The vibrational free energy of the defective and perfect systems is estimated with the quasiharmonic formula [22–25]

$$F^{\mathrm{qh}}(\eta, T) = \frac{1}{N_q} k_B T \sum_{\mathbf{q}s} \ln\left[2\sinh\left(\frac{\hbar\omega_{\mathbf{q}s}(\eta)}{2k_B T}\right)\right], \qquad (2)$$

where N_q is the total number of wave vectors used for integration within the Brillouin zone (BZ), and the dependence of the phonon frequencies, $\omega_{\boldsymbol{q}s}$, on epitaxial strain is explicitly noted.

It is well known that estimations of μ_{O} using DFT with the Hubbard U parameter methods may contain large errors [26,27]. This inherent limitation makes the prediction of accurate reduction temperatures impractical when using standard DFT approaches only. Notwithstanding, since (i) the oxygen chemical potential does not depend on epitaxial strain (i.e., μ_{O} is a property of the gas which depends on temperature and density) and (ii) we are mainly concerned with unraveling the fundamental effects of the lattice excitations on V_{O} formation as a function of η, we can safely base our following analysis on the results obtained for the thermodynamically shifted Gibbs free energy:

$$G^{*\mathrm{qh}}_{\mathrm{vac}}(\eta, T) = G^{\mathrm{qh}}_{\mathrm{vac}}(\eta, T) - \mu_{\mathrm{O}}(T). \qquad (3)$$

In other words, rather than trying to adopt experimental values for μ_{O} and applying empirical corrections to the calculated vacancy-formation energies (i.e., as is customarily done when trying to predict reasonable reduction temperatures [15,27]—which is beyond our present scope), we arbitrarily set the oxygen gas chemical potential to zero.

B. Computational details

We use the generalized-gradient approximation of DFT due to Perdew, Burke, and Ernzerhof [28], as implemented in the Vienna *ab initio* simulation package (VASP) [29]. A "Hubbard-U" scheme [30] is employed for a better treatment of Co's ($U = 6.0$ eV in $SrCoO_3$ [31] and 4.0 eV in $La_{0.5}Sr_{0.5}Mn_{0.5}Co_{0.5}O_3$ [32] thin films) and Mn's ($U = 3.3$ eV [32]) $3d$ electrons. We use the "projector-augmented-wave" method [33] to represent the ionic cores, considering the following electrons as valence states: Sr's $4s$, $4p$, and $5s$; Co's $3p$, $4s$, and $3d$; La's $5s$, $5p$, $5d$, and $6s$; Mn's $3p$, $4s$, and $3d$; and O's $2s$ and $2p$. Wave functions are represented in a plane-wave basis truncated at 600 eV. For the determination of equilibrium geometries, we use a 20-atom simulation cell that allows us to reproduce the usual ferroelectric and antiferrodistortive distortions in perovskite oxides [34] [see Fig. 1(b)]. Defective configurations are generated by removing one oxygen atom in either an equatorial (eq) or an apical (ap) position, which corresponds to the case $\delta = 0.25$. For integrations in the BZ, we employ a Γ-centered $\mathbf{k}$-point grid of $6 \times 6 \times 6$. Geometry relaxations are performed by using a conjugate-gradient algorithm that changes the volume and the shape of the unit cell (while fulfilling the lattice vector constraints required to simulate thin films), and the imposed tolerance

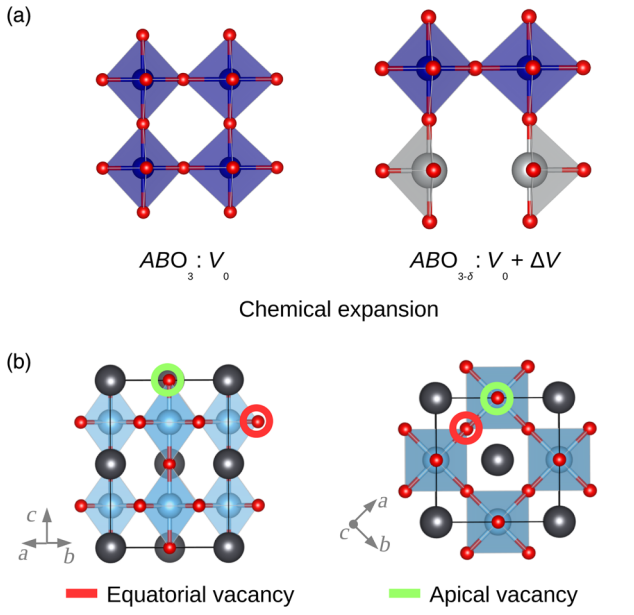

FIG. 1. (a) Sketch of the chemical expansion occurring in bulk ABO_3 perovskites due to oxygen reduction. (b) The 20-atom $\sqrt{2} \times \sqrt{2} \times 2$ simulation cell used in our zero-temperature energy calculations; red, blue, and black spheres represent the O, B, and A atoms, respectively. Equatorial and apical oxygen positions are noted in the figure.

on the atomic forces is 0.01 eV/Å. We identify the crystal symmetry of the final equilibrium structures with the ISOTROPY package [35]. By using these parameters, we obtain total energies that are converged to within 0.5 meV per formula unit.

For our phonon-frequency calculations, we employ the so-called direct approach [36], in which the force-constant matrix of the crystal is directly calculated in real space by considering the proportionality between atomic displacements and forces when the former are sufficiently small (in the present case, this condition is satisfied when the atomic displacements are of 0.02 Å). Large supercells containing 160 atoms are employed for guaranteeing that the elements of the force-constant matrix all fall off to negligible values at their boundaries, a condition that follows from the use of periodic boundary conditions. We use a dense **k**-point grid of $3 \times 3 \times 3$ for the calculation of the atomic forces with VASP. The computation of the nonlocal parts of the pseudopotential contributions is performed in reciprocal space in order to maximize our numerical accuracy. Once the force-constant matrix of the system is determined, we Fourier transform it to obtain the phonon frequencies at any **k** point contained in the BZ. The latter step is performed with the PHON code [36], in which we exploit the translational invariance of the system to impose that the three acoustic branches are exactly zero at the Γ point and use central differences for the atomic forces (i.e., we consider both positive and negative atomic displacements). A complete phonon calculation involves the evaluation of atomic forces in 120 (114) different stoichiometric (nonstoichiometric) configurations with the technical parameters just described. In order to compute $F_{\mathrm{vac}}^{\mathrm{qh}}$, we employ a dense **k**-point grid of $16 \times 16 \times 16$ for BZ sampling. With these settings, we find that the calculated quasiharmonic free energies are accurate to within 5 meV per formula unit.

It is worth noticing that all of the analyzed systems are found to be vibrationally stable; that is, none of them exhibit imaginary phonon frequencies (for some examples, see Fig. 2). In the specific case of SCO thin films, we note that the vibrational phonon spectrum calculated at zero strain [Fig. 2(a)] is practically identical to the one estimated for the corresponding bulk system (see Fig. 6 in Ref. [31]), essentially due to the tetragonal symmetry of the crystal.

III. RESULTS AND DISCUSSION

A. $SrCoO_{3-\delta}$ thin films

According to our DFT calculations, the ground state of stoichiometric SCO is a tetragonal $P4/mbm$ phase with an equilibrium lattice parameter of $a_0 = 3.89$ Å and ferromagnetic (FM) spin ordering [31]. At $\eta \sim +2\%$, the system undergoes a magnetic phase transition to an antiferromagnetic state displaying C-type spin ordering [i.e., spins in the plane parallel to the substrate align antiparallel, whereas spins in planes perpendicular to the substrate align parallel; see Fig. 3(a)]. In the presence of oxygen vacancies, the magnetic properties of SCO change noticeably: The ground state becomes G-type antiferromagnetic [i.e., spins align antiparallel both in the substrate plane and perpendicular to it; see Fig. 3(b)] either at moderately tensile or compressive (negative) strains. With regard to E_{vac}, we find that

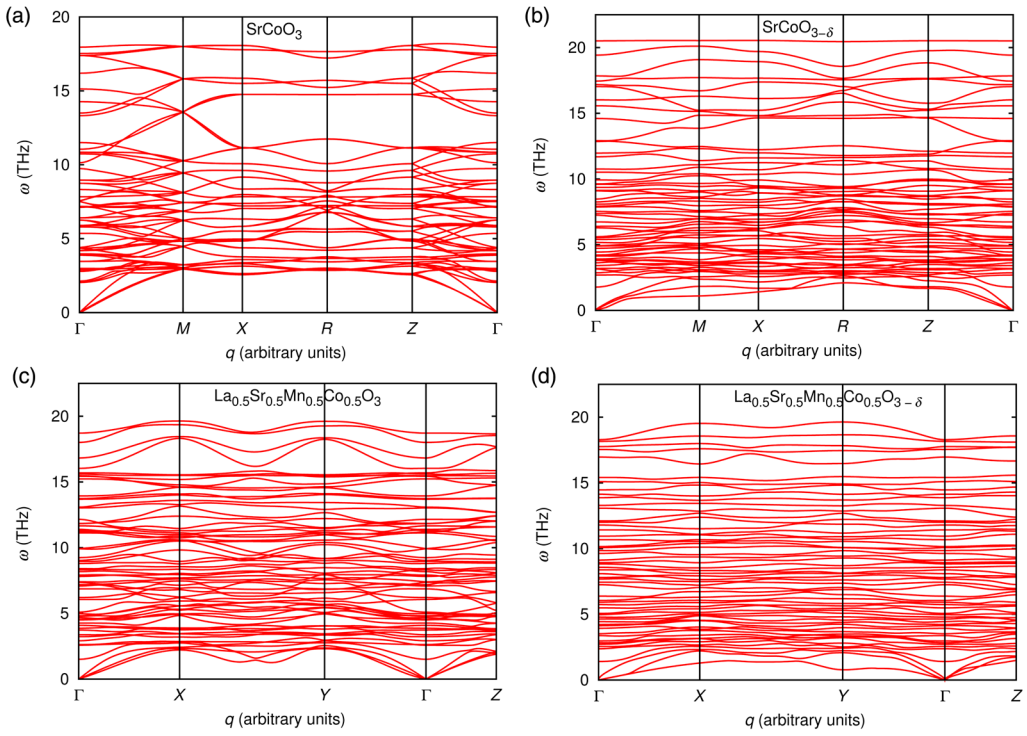

FIG. 2. Vibrational phonon spectrum calculated in (a) a stoichiometric $SrCoO_3$ thin film with the in-plane lattice parameter $a = 3.89$ Å, (b) a nonstoichiometric $SrCoO_{3-\delta}$ ($\delta = 0.25$) thin film with the in-plane lattice parameter $a = 3.89$ Å, (c) a stoichiometric $La_{0.5}Sr_{0.5}Mn_{0.5}Co_{0.5}O_3$ thin film with the in-plane lattice parameter $a = 3.90$ Å, and (d) a nonstoichiometric $La_{0.5}Sr_{0.5}Mn_{0.5}Co_{0.5}O_{3-\delta}$ ($\delta = 0.25$) thin film with the in-plane lattice parameter $a = 3.90$ Å.

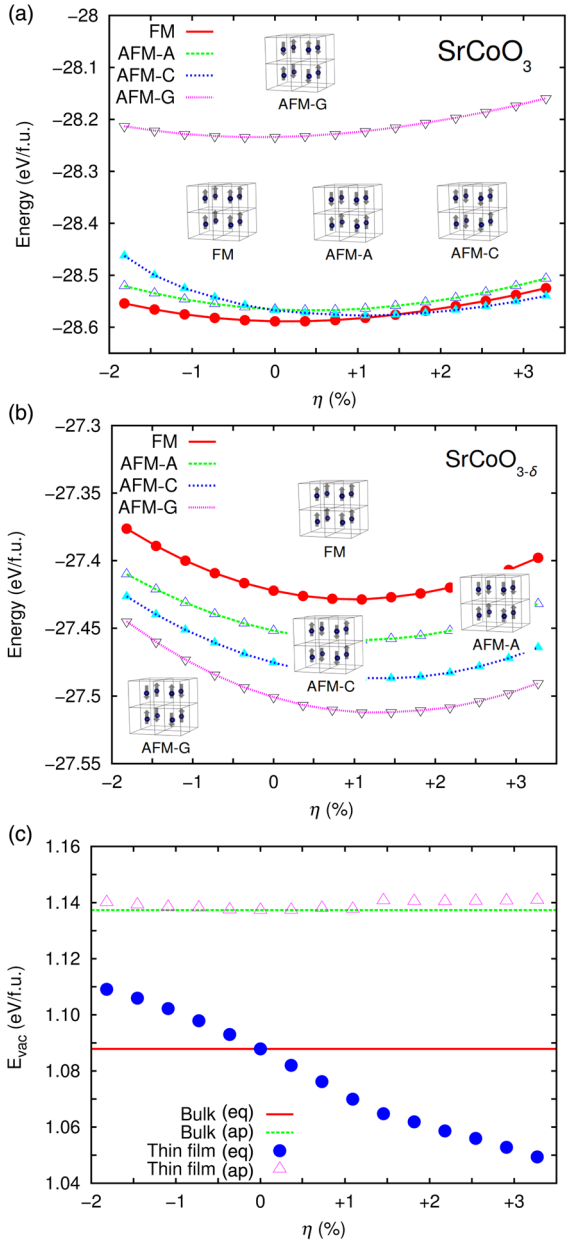

FIG. 3. Zero-temperature calculations done in perfect and nonstoichiometric ($\delta = 0.25$) SCO thin films. (a),(b) Total energy results expressed as a function of magnetic spin ordering, epitaxial strain, and oxygen content. (c) The zero-temperature vacancy-formation energy. Both equatorial (eq) and apical (ap) oxygen-vacancy positions are considered, and analogous results obtained in bulk are shown for comparison purposes.

(at $T = 0$) equatorial vacancies can be created more easily than apical vacancies [i.e., $E_{\mathrm{vac}}(\mathrm{ap}) - E_{\mathrm{vac}}(\mathrm{eq}) \sim 10$ meV/formula unit (f.u.)] and that their formation energy decreases almost linearly with increasing strain [Fig. 3(c)]. For instance, at $\eta = +2\%$, the (eq) vacancy formation energy is reduced by 30 and 52 meV/f.u. compared to the unstrained and -2% cases, respectively. We note that these zero-temperature results are consistent with those reported by Hu *et al.* [14] and Tahini *et al.* [17] in analogous systems, and by Aschauer *et al.* [15] in $CaMnO_3$ thin films.

In view of the outcomes shown in Fig. 3(c), one might guess that, provided that the thermal contributions to V_O formation are more or less independent of epitaxial strain, tensile strain should favor the formation of vacancies at $T \neq 0$ conditions. However, as we have noted, this is not what was observed experimentally by Hu *et al.* in $SrCoO_{3-\delta}$ thin films [14]. Figure 4(a) shows our vibrational-entropy results obtained for an equatorial vacancy, $F_{\mathrm{vac}}^{\mathrm{qh}}$, under compressive, neutral, and tensile strains expressed as a function of temperature; the following conclusions can be drawn from them. First, vibrational contributions to the V_O free energy strongly depend on the epitaxial strain; in the specific case of SCO, those contributions are most favorable in compressive thin films, contrary to what is found for E_{vac}. Second, at $T \approx 300$ K, the $F_{\mathrm{vac}}^{\mathrm{qh}}$ difference between various η states can be on the same order of magnitude, in absolute value, as the corresponding E_{vac} difference calculated at $T = 0$. For example, at room temperature, the vibrational vacancy entropy estimated at $\eta = -2\%$ is 16 and 49 meV/f.u. smaller than that obtained in the unstrained and $+2\%$ cases, respectively. These findings imply that, as temperature is steadily increased, lattice excitations may

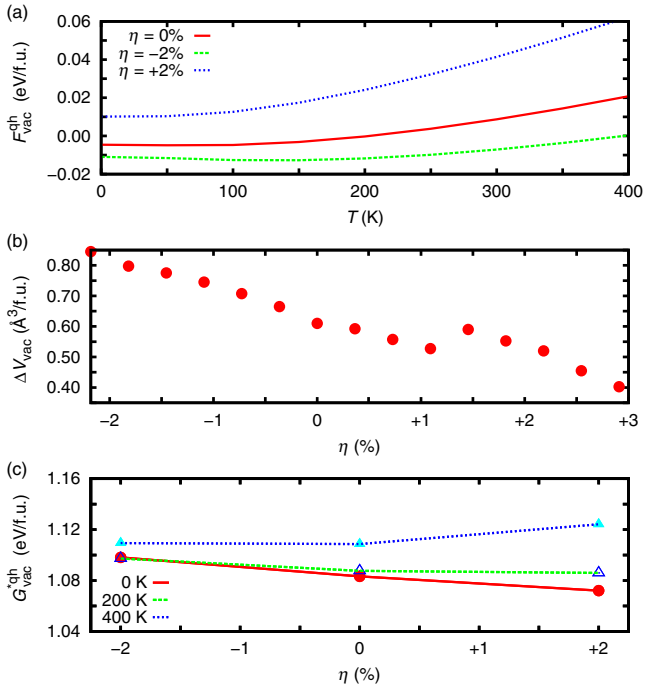

FIG. 4. Quasiharmonic free-energy calculations performed in perfect and nonstoichiometric ($\delta = 0.25$, equatorial vacancies) SCO thin films. (a) Vibrational and (c) thermodynamically shifted Gibbs vacancy free-energy results expressed as a function of temperature and epitaxial strain. (b) The accompanying chemical expansion, ΔV_{vac}, expressed as a function of epitaxial strain.

entirely reverse the vacancy-formation trends deduced at zero temperature. This effect is explicitly shown in Fig. 4(c), where, at the highest considered temperature, it is easiest to create oxygen vacancies in compressively strained thin films; that is, $G^{*\mathrm{qh}}_{\mathrm{vac}}$ is at minimum at $\eta = -2\%$. (For analogous quasiharmonic Gibbs free energy V_{O} results obtained at room temperature, the interested reader is referred to Ref. [14].)

In Fig. 4(b), we enclose the chemical-expansion results, $\Delta V_{\mathrm{vac}}(\eta) \equiv V_{\mathrm{SrCoO}_{3-\delta}}(\eta) - V_{\mathrm{SrCo}}(\eta)$, obtained in SCO thin films. We note that, in this case, the change in volume corresponds to an increase of the unit cell along the out-of-plane direction, rather than to an isotropic volume expansion as it occurs in bulk, since η (or, equivalently, the in-plane lattice parameter a) is considered to be the same in both stoichiometric and nonstoichiometric thin films. It is found that ΔV_{vac} is largest at compressive strains, and a small kink appears at the point at which the stoichiometric system undergoes a magnetic phase transition. As the vibrational properties of crystals depend largely on volume [i.e., the V dependence of the phonon frequencies, $\omega_{\boldsymbol{q}s}$, normally can be described with the Grüneisen parameter $\gamma_{\boldsymbol{q}s} = -\partial(\ln \omega_{\boldsymbol{q}s})/\partial(\ln V)$], we can reasonably correlate the observed $F^{\mathrm{qh}}_{\mathrm{vac}}$ dependence on strain to the accompanying chemical expansion: The larger the ΔV_{vac}, the more favorable the lattice contributions to V_{O} formation are. We comment again on this point below.

B. $La_{0.5}Sr_{0.5}Mn_{0.5}Co_{0.5}O_{3-\delta}$ thin films

Our DFT calculations predict an orthorhombic *Pbnm* ground state for bulk stoichiometric LSMCO that is characterised by FM spin ordering and oxygen octahedral rotations $(a^-a^-a^+)$, as expressed in Glazer's notation [37] (i.e., antiphase within the substrate plane and in phase in the perpendicular direction). At a tensile epitaxial strain of about $+1\%$ (where $a_0 = 3.90$ Å), the system undergoes a first-order transition to a monoclinic (and centrosymmetric) $P2/m$ phase, characterized also by FM spin ordering and O_6 rotations $(a^-a^-a^0)$ [i.e., octahedral tiltings along the direction perpendicular to the substrate disappear; see Fig. 5(a)]. In the presence of oxygen vacancies, the magnetic properties of LSMCO thin films remain invariant. With regard to E_{vac}, we also find that (at $T = 0$) equatorial vacancies are created more easily than apical vacancies [i.e., $E_{\mathrm{vac}}(\mathrm{ap}) - E_{\mathrm{vac}}(\mathrm{eq}) \sim 10$ meV/f.u.], although the corresponding formation energy in this case is quite insensitive to the strain conditions [Fig. 5(b)].

Figure 6(a) shows our vibrational-entropy results obtained for an equatorial vacancy, $F^{\mathrm{qh}}_{\mathrm{vac}}$, under compressive, neutral, and tensile strains expressed as a function of temperature. It is observed that lattice contributions to V_{O} formation now are practically identical in the $\eta = 0$ and -2% cases, and that $F^{\mathrm{qh}}_{\mathrm{vac}}$ is smallest for tensile strains.

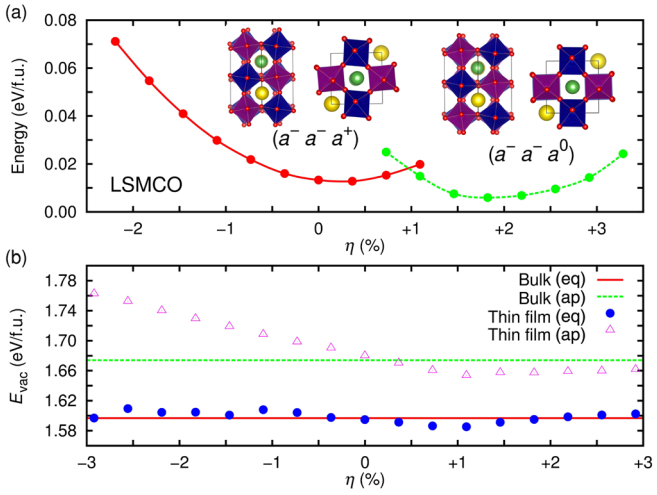

FIG. 5. Zero-temperature calculations done in perfect and nonstoichiometric ($\delta = 0.25$) LSMCO thin films. (a) Total energy results obtained in stoichiometric systems expressed as a function of epitaxial strain. (b) The zero-temperature vacancy-formation energy. Both equatorial (eq) and apical (ap) oxygen-vacancy positions are considered, and analogous results obtained in bulk are shown for comparison.

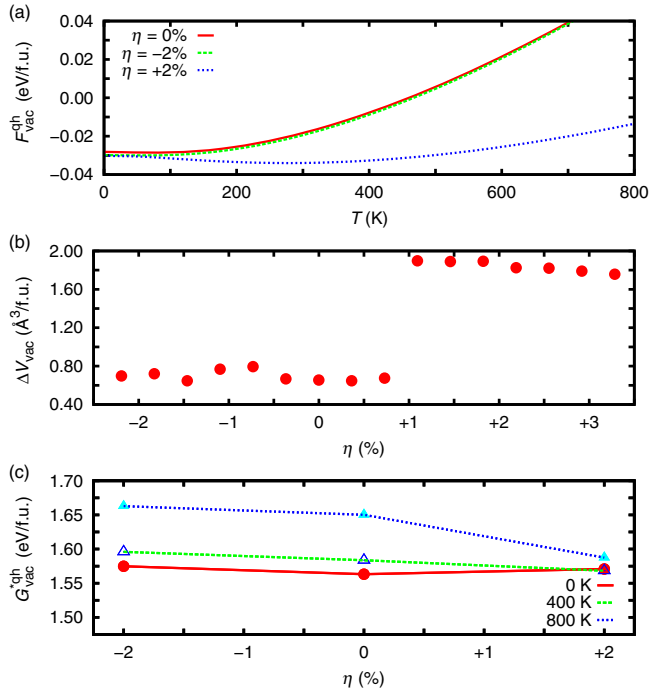

FIG. 6. Quasiharmonic free-energy calculations performed in perfect and nonstoichiometric ($\delta = 0.25$, equatorial vacancies) LSMCO thin films. (a) Vibrational and (c) thermodynamically shifted Gibbs vacancy free-energy results expressed as a function of temperature and epitaxial strain. (b) The accompanying chemical expansion, ΔV_{vac}, expressed as a function of epitaxial strain.

This behavior suggests that, at finite temperatures, equatorial vacancies in LSMCO thin films will be created more easily at $\eta > 0$ conditions, as is explicitly shown in Fig. 6(c), essentially due to lattice effects. In this case, we also find that the chemical expansion of the crystal [Fig. 6(b)] and vibrational vacancy entropy are strongly correlated. Specifically, the $\Delta V_{\rm vac}$ values computed in the $\eta = 0$ and -2% cases are almost identical, and so are the corresponding $F^{\rm qh}_{\rm vac}$ curves. Meanwhile, the chemical expansion is larger at tensile strains due to the underlying $Pbnm \rightarrow P2/m$ phase transition occurring at $\eta \sim +1\%$, and, simultaneously, the vibrational vacancy entropy becomes more favorable. Therefore, our *ab initio* results obtained in SCO and LSMCO thin films evidence a direct link between the quantities $\Delta V_{\rm vac}$ and $F^{\rm qh}_{\rm vac}$.

C. Oxygen-vacancy ordering

It was recently suggested, based on the outcomes of zero-temperature $E_{\rm vac}$ calculations, that epitaxial strain could be used as a means to engineer vacancy ordering in perovskite oxides [15]. In fact, this appears to be the logical conclusion resulting from Figs. 3(c) and 5(b) when intervacancy interactions are disregarded [15]. However, as we have already shown, T-induced lattice vibrations can play a critical role in the formation of oxygen vacancies in thin films.

In order to quantify the effects of lattice excitations on possible vacancy ordering, we calculate the vibrational entropy of apical (ap) vacancies in SCO thin films considering different strain states [see Fig. 7(a)]. It is found that the $F^{\rm qh}_{\rm vac}$ energies obtained for ap vacancies qualitatively follow the same trends as eq vacancies; namely, vibrational contributions to the free energy tend to favor the formation of $V_{\rm O}$ at compressive conditions (i.e., $\eta < 0$). However, the $F^{\rm qh}_{\rm vac}$ values obtained for ap vacancies are systematically smaller than those obtained for eq, and the estimated $F^{\rm qh}_{\rm vac}({\rm ap}) - F^{\rm qh}_{\rm vac}({\rm eq})$ differences may be comparable in absolute value to the corresponding static differences $E_{\rm vac}({\rm ap}) - E_{\rm vac}({\rm eq})$. For instance, at $\eta = -2\%$ and $T = 600$ K, the vibrational entropy of ap vacancies is about 25 meV/f.u. smaller than that of eq, and, consequently, $G^{*{\rm qh}}_{\rm vac}({\rm ap}) \approx G^{*{\rm qh}}_{\rm vac}({\rm eq})$. Lattice vibrations, therefore, may hinder point-defect ordering in SCO thin films as to a fine approximation (that is, by neglecting possible intervacancy interactions [15]), the equilibrium ratio of eq to ap vacancies is approximately 1. In $La_{0.5}Sr_{0.5}Mn_{0.5}Co_{0.5}O_{3-\delta}$ thin films [see Fig. 7(b)], we also find that lattice excitations favor the formation of ap vacancies over eq —although, in this case, at medium and high temperatures (i.e., $T > 210$ K)—and that they tend to prevent vacancy ordering. For instance, in $\eta = 0\%$ thin films, the static formation-energy difference between eq and ap vacancies is $\Delta E_{\rm vac} = E_{\rm vac}({\rm ap}) - E_{\rm vac}({\rm eq}) = 80\,{\rm meV/f.u.}$, whereas, at $T \geq 850$ K, the corresponding vibrational free-energy difference is $\Delta F^{\rm qh}_{\rm vac} = F^{\rm qh}_{\rm vac}({\rm ap}) - F^{\rm qh}_{\rm vac}({\rm eq}) \leq -80\,{\rm meV/f.u.}$ Consequently, $G^{*{\rm qh}}_{\rm vac}({\rm ap}) \approx G^{*{\rm qh}}_{\rm vac}({\rm eq})$ at elevated temperatures.

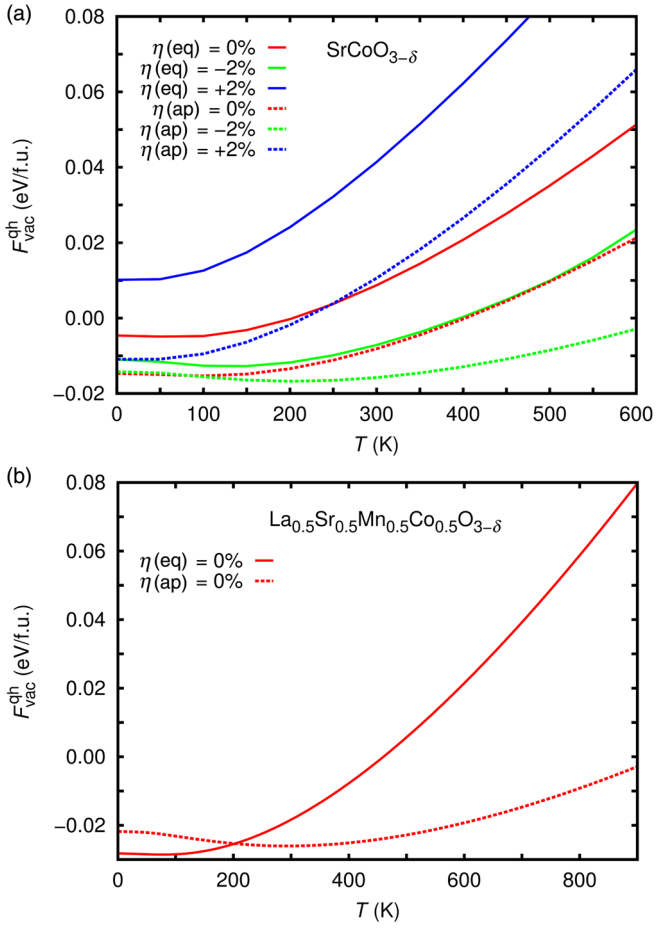

FIG. 7. Quasiharmonic vibrational free energy of equatorial (eq, solid lines) and apical (ap, dashed lines) oxygen vacancies calculated in (a) $SrCoO_{3-\delta}$ ($\delta = 0.25$) and (b) $La_{0.5}Sr_{0.5}Mn_{0.5}Co_{0.5}O_{3-\delta}$ ($\delta = 0.25$) thin films, expressed as a function of temperature and epitaxial strain, η.

Finally, we note that the configurational entropy of point defects always favor the formation of eq vacancies over that of ap in perovskite oxides, namely, $\Delta F^{\rm conf}_{\rm vac} = F^{\rm conf}_{\rm vac}({\rm ap}) - F^{\rm conf}_{\rm vac}({\rm eq}) = \delta k_B T \ln(2)$. However, at high-enough temperatures, the impact of T-induced disorder mostly can be regarded as secondary, namely, $|\Delta F^{\rm conf}_{\rm vac}| \ll |\Delta F^{\rm qh}_{\rm vac}|$ (see Fig. 7).

IV. CONCLUSIONS

In this work, we show that lattice vibrations play a critical role in the formation of oxygen vacancies in perovskite thin films. The dependence of the vibrational vacancy entropy on epitaxial strain appears to be system dependent, and it can be strongly influenced by underlying phase transitions. Nevertheless, we reveal a direct link

between $F_{\mathrm{vac}}^{\mathrm{qh}}$ and the chemical expansion of the thin film, ΔV_{vac}, which can be straightforwardly used in standard $T = 0$ calculations to qualitatively foresee the effects of thermal excitations on V_{O} formation. In the two perovskite oxides analyzed in this work, lattice vibrations tend to be the opposite of oxygen-vacancy ordering. Consideration of thermal lattice excitations, therefore, appears to be necessary for describing the latter effect correctly.

ACKNOWLEDGMENTS

The author wishes to thank N. A. Katcho for stimulating discussions. This research was supported by the Australian Research Council under the Future Fellowship funding scheme (Grant No. FT140100135). Computational resources and technical assistance were provided by the Australian Government and the Government of Western Australia through Magnus under the National Computational Merit Allocation Scheme and The Pawsey Supercomputing Centre.

[1] Z. Shao and M. H. Sossina, A high-performance cathode for the next generation of solid-oxide fuel cells, Nature (London) **431**, 170 (2004).

[2] H. Jeen, W. S. Choi, M. D. Biegalski, C. M. Folkman, I.-C. Tung, D. D. Fong, J. W. Freeland, D. Shin, H. Ohta, M. F. Chisholm, and H. N. Lee, Reversible redox reactions in an epitaxially stabilized $SrCoO_x$ oxygen sponge, Nat. Mater. **12**, 1057 (2013).

[3] N. Tsvetkov, Q. Lu, L. Sun, E. J. Crumlin, and B. Yildiz, Improved chemical and electrochemical stability of perovskite oxides with less reducible cations at the surface, Nat. Mater. **15**, 1010 (2016).

[4] H. Taguchi, M. Shimada, and M. Koizumi, The effect of oxygen vacancy on the magnetic properties in the system $SrCoO_{3-\delta}$ $(0 < \delta < 0.5)$, J. Solid State Chem. **29**, 221 (1979).

[5] J. B. Goodenough, Electronic and ionic transport properties and other physical aspects of perovskites, Rep. Prog. Phys. **67**, 1915 (2004).

[6] D. Cao, M. Q. Cai, Y. Zheng, and W. Y. Hu, First-principles study for vacancy-induced magnetism in nonmagnetic ferroelectric $BaTiO_3$, Phys. Chem. Chem. Phys. **11**, 10934 (2009).

[7] S. B. Adler, Chemical expansivity of electrochemical ceramics, J. Am. Ceram. Soc. **84**, 2117 (2001).

[8] H. Ullmann and N. Trofimenko, Estimation of effective ionic radii in highly defective perovskite-type oxides from experimental data, J. Alloys Compd. **316**, 153 (2001).

[9] D. Marrocchelli, N. H. Perry, and S. R. Bishop, Understanding chemical expansion in perovskite-structured oxides, Phys. Chem. Chem. Phys. **17**, 10028 (2015).

[10] D. S. Aidhy, B. Liu, Y. Zhang, and W. J. Weber, Chemical expansion affected oxygen vacancy stability in different oxide structures from first principles calculations, Comput. Mater. Sci. **99**, 298 (2015).

[11] S. Hu, Z. Yue, J. S. Lim, S. J. Callori, J. Bertinshaw, A. Ikeda-Ohno, T. Ohkochi, C. H. Yang, X. Wang, C. Ulrich, and J. Seidel, Growth and properties of fully strained $SrCoO_x$ $(x \simeq 2.8)$ thin films on $DyScO_3$, Adv. Mater. Interfaces **2**, 1500012 (2015).

[12] J. R. Petrie, C. Mitra, H. Jeen, W. S. Choi, T. L. Meyer, F. A. Reboredo, J. W. Freeland, G. Eres, and H. N. Lee, Strain control of oxygen vacancies in epitaxial strontium cobaltite films, Adv. Funct. Mater. **26**, 1564 (2016).

[13] P. Agrawal, J. Guo, C. Hébert, D. Passerone, R. Erni, and M. D. Rosell, Strain-driven oxygen deficiency in multiferroic $SrMnO_3$ thin films, Phys. Rev. B **94**, 104101 (2016).

[14] S. Hu, Y. Wang, C. Cazorla, and J. Seidel, Strain-enhanced oxygen dynamics and redox reversibility in topotactic $SrCoO_{3-\delta}$ $(0 < \delta < 0.5)$, Chem. Mater. **29**, 708 (2017).

[15] U. Aschauer, R. Pfenninger, S. M. Selbach, T. Grande, and N. A. Spalding, Strain-controlled oxygen vacancy formation and ordering in $CaMnO_3$, Phys. Rev. B **88**, 054111 (2013).

[16] U. Aschauer, N. Vonrüti, and N. A. Spalding, Effect of epitaxial strain on cation and anion vacancy formation in MnO, Phys. Rev. B **92**, 054103 (2015).

[17] H. A. Tahini, X. Tan, U. Schwingenschlögl, and S. C. Smith, Formation and migration of oxygen vacancies in $SrCoO_3$ and their effect on oxygen evolution reactions, ACS Catal. **6**, 5565 (2016).

[18] C. L. Flint, A. J. Grutter, C. A. Jenkins, E. Arenholz, and Y. Suzuki, Magnetism in $CaMnO_3$ thin films, J. Appl. Phys. **115**, 17D712 (2014).

[19] T. Takeda and H. Watanabe, Magnetic properties of the system $SrCo_{1-x}Fe_xO_{3-y}$, J. Phys. Soc. Jpn. **33**, 973 (1972).

[20] H. Jeen, W. S. Choi, J. W. Freeland, H. Ohta, C. U. Jung, and H. N. Lee, Topotactic phase transformation of the brownmillerite $SrCoO_{2.5}$ to the perovskite $SrCoO_{3-\delta}$, Adv. Mater. **25**, 3651 (2013).

[21] A. Aguadero, H. Falcon, J. M. Campos-Martín, S. M. Al-Zahrani, J. L. G. Fierro, and J. A. Alonso, An oxygen-deficient perovskite as selective catalyst in the oxidation of alkyl benzenes, Angew. Chem., Int. Ed. Engl. **50**, 6557 (2011).

[22] C. Cazorla and J. Íñiguez, Insights into the phase diagram of bismuth ferrite from quasiharmonic free-energy calculations, Phys. Rev. B **88**, 214430 (2013).

[23] C. Cazorla, D. Errandonea, and E. Sola, High-pressure phases, vibrational properties, and electronic structure of $Ne(He)_2$ and $Ar(He)_2$: A first-principles study, Phys. Rev. B **80**, 064105 (2009).

[24] C. Cazorla and J. Boronat, First-principles modeling of quantum nuclear effects and atomic interactions in solid ^{4}He at high pressure, Phys. Rev. B **91**, 024103 (2015).

[25] S. Baroni, P. Giannozzi, and E. Isaev, Density-functional perturbation theory for quasi-harmonic calculations, Rev. Mineral. Geochem. **71**, 39 (2010).

[26] R. O. Jones and O. Gunnarsson, The density functional formalism, its applications and prospects, Rev. Mod. Phys. **61**, 689 (1989).

[27] L. Wang, T. Maxisch, and G. Ceder, Oxidation energies of transition metal oxides within the GGA + U framework, Phys. Rev. B **73**, 195107 (2006).

[28] J. P. Perdew, K. Burke, and M. Ernzerhof, Generalized Gradient Approximation Made Simple, Phys. Rev. Lett. **77**, 3865 (1996).

[29] G. Kresse and J. Fürthmuller, Efficient iterative schemes for *ab initio* total-energy calculations using a plane-wave basis set, Phys. Rev. B **54**, 11169 (1996).

[30] S. L. Dudarev, G. A. Botton, S. Y. Savrasov, C. J. Humphreys, and A. P. Sutton, Electron-energy-loss spectra and the structural stability of nickel oxide: An LSDA + U study, Phys. Rev. B **57**, 1505 (1998).

[31] P. Rivero and C. Cazorla, Revisiting the zero-temperature phase diagram of stoichiometric $SrCoO_3$ with first-principles methods, Phys. Chem. Chem. Phys. **18**, 30686 (2016).

[32] Y.-L. Lee, M. J. Gadre, Y. Saho-Horn, and D. Morgan, *Ab initio* GGA + U study of oxygen evolution and oxygen reduction electrocatalysis on the (001) surfaces of lanthanum transition metal perovskites $LaBO_3$ (B = Cr, Mn, Fe, Co and Ni), Phys. Chem. Chem. Phys. **17**, 21643 (2015).

[33] P. E. Blöchl, Projector augmented-wave method, Phys. Rev. B **50**, 17953 (1994).

[34] C. Cazorla and M. Stengel, Electrostatic engineering of strained ferrorelectric perovskites from first-principles, Phys. Rev. B **92**, 214108 (2015).

[35] H. T. Stokes and D. M. Hatch, FINDSYM: Program for identifying the space group symmetry of a crystal, J. Appl. Crystallogr. **38**, 237 (2005); H. T. Stokes, D. M. Hatch, and B. J. Campbell, ISOTROPY, http://stokes.byu.edu/isotropy.html (2007).

[36] D. Alfè, PHON: A program to calculate phonons using the small displacement method, Comput. Phys. Commun. **180**, 2622 (2009).

[37] A. Glazer, The classification of tilted octahedra in perovskites, Acta Crystallogr. Sect. B **28**, 3384 (1972).